We are IntechOpen,
the world's leading publisher of
Open Access books
Built by scientists, for scientists

4,400
Open access books available

117,000
International authors and editors

130M
Downloads

Our authors are among the

154
Countries delivered to

TOP 1%
most cited scientists

12.2%
Contributors from top 500 universities

BOOK CITATION INDEX
CLARIVATE ANALYTICS
INDEXED

WEB OF SCIENCE™

Selection of our books indexed in the Book Citation Index
in Web of Science™ Core Collection (BKCI)

Interested in publishing with us?
Contact book.department@intechopen.com

Numbers displayed above are based on latest data collected.
For more information visit www.intechopen.com

Electric Drives in Alternative Fuel Vehicles — Some New Definitions and Methodologies

Xi Zhang

Additional information is available at the end of the chapter

Abstract

This chapter focuses on some new definitions and methodologies of electric drives that are facing new challenges raised by alternative fuel vehicles. It starts with the objectives, fundamentals, and current research issues of alternative fuel vehicles based electric drives, before moving on to new definitions of unified modeling of the entire electric drive system and design of the proposed DC active power filter aimed at energy storage system chaotic current elimination. Next, novel motor control strategies taking into account alternative fuel vehicle operations are presented for improvement of sensorless drive and flux weakening control performance. Finally, conclusions of this chapter are drawn.

Keywords: Alternative fuel vehicles, unified modeling, DC active power filter, sliding mode observer, flux weakening control

1. Introduction

1.1. Electric drive application background in Alternative Fuel Vehicles (AFVs)

The current worldwide energy shortage and unbalanced distribution is becoming increasingly serious, and resource competition is getting fierce. The potential petroleum resources gradually decline, while global oil consumption continues to increase. Traditional Automobiles have to face an unprecedented impact and challenges. On the other hand, with the traditional automobile production sharply increasing, environmental impact becomes more apparent. The emissions of CO_2 and other greenhouse gases and global warming [1] come into our view. Alternative fuel vehicles (AFVs) are gradually becoming an inevitable choice for all countries

to innovate the automobile industry. For instance, in the United States, the sales volume of battery electric vehicles (BEVs) is expected to account for 12% of that of all registered vehicles in 2025. As an energy-efficient, low-carbon and environment friendly traffic tool, AFVs are expected to become increasingly popular in the future.

Most national research institutions and automobile manufacturers have increased R&D investment in the AFV technology to replace traditional vehicles, forming the trend of different technologies developed in parallel. Some of the technologies have achieved significant success in commercial fields [2], [3]. In the United States, Germany, and Japan, GM, Ford, Volkswagen, BMW, Toyota, Honda, and other major automobile manufacturers have adopted different new technology development strategies, based on the situation of the nation and the company, and successfully developed a number of concept AFVs and utility vehicles. AFVs are usually classified into hybrid electric vehicles (HEVs), electric vehicles (EVs), fuel cell electric vehicles (FCEVs).

Some countries, e.g., Japan, have been committed to the hybrid vehicles and have developed a lot of well-known models, e.g., the Toyota "Prius." Some other countries, e.g., Germany, have unique technology in the pure electric vehicles, fuel cell electric vehicles, and so on. BMW i3 with carbon fiber body is the lightest electric car on the market.

The world's major automobile production countries have policies to promote the development of AFVs to cope with difficulties and opportunities. By 2015, the United States raised the goal to one million plug-in hybrid electric vehicles (PHEVs). Tax incentives have been implemented. The EU will issue €7 billion loan to support energy-efficient vehicles. The German government raised million BEV and PHEV goals by 2020. Japan in 2009 proposed a "carbon revolution" program, in which development of electric vehicles is one of the core. In China, basic research and the establishment of public service platform are listed as the focus of development. "Three vertical and three horizontal" development layout is presented to promote the AFV industries.

1.2. Current research situation and new challenges for electric drives in AFVs

AFV electric drive systems include the energy storage systems (battery and/or ultracapacitor), electronic controller, power converters, motors, and so on. The electronic controller is divided into three functional units: sensors, circuits, and processors. In driving and regenerative processes, the energy flow between the energy source and the motor is adjusted by the power converter.

The electric drive system itself as a whole is closely linked with the energy subsystem, which is the core technology of electric vehicles. The main function of electric drive system is to transfer energy from storage system to wheels, which is used for overcoming rolling resistance, air resistance, acceleration resistance, and climbing resistance. When braking, the mechanical energy is converted to electrical energy back to the energy storage system. AFVs can choose single or dual motor drives. AFVs can also employ in-wheel motors. Now, low-power electric vehicles on the market almost all employ single-motor power systems with simple structure.

However, high-power electric vehicles such as electric buses generally use dual motor powered system. AC drives can be divided into induction motor drive system and synchronous motor drive system. Synchronous motor drive systems can be classified as permanent magnet synchronous motor drive system (PMSM Drives) and switched reluctance motor (SRM) drive system. Currently, the commercial application of power systems for electric vehicles is divided into three categories: the DC motor drive system, induction motor drive system, and permanent magnet synchronous motor drive system. Representative products include "Peugeot 106 EV" (DC motor), "General EVI" (induction motor), and "Honda EV Plus" (permanent magnet synchronous motor), respectively. With the development of power electronics, micro-electronics, and control technology, the digital AC drive systems (IM Drives and PMSM Drives) are widely applied in commercial AFVs.

A 3-phase 4-pole induction motor and an electronics module with 72 IGBTs are adopted by the famous electric car Tesla Model S. The efficiency of the battery pack, power electronics modules, and motor system can reach 85–95%. It weighs only 70 pounds, can generate large torque at very low speed, and the max motor speed could be 13,000 rpm, which cannot be done by the internal combustion engine.

At present, there are still disadvantages in the electric drive system. First, the long charging times, which usually exceed 30 minutes [4] for a full charge, as well as the range limitation of EVs due to the available battery technologies, are still challenging problems.

Short driving distance, greatly limits the application and development of electric vehicles. In electric vehicles, the power supply did no progress a lot. Effective use of the vehicle power supply energy is an urgent problem. Torque of the drive motor, speed control accuracy, and efficiency optimization requires improvement over the entire range.

The motor runs under bad conditions, e.g., the vehicle engine vibration and high-temperature environment. Therefore, the motor must be adapted to environmental conditions: reliable, stable, and safe operation. Due to space limitations, high-density, compact, and lightweight motors are in need.

1.3. Objectives and contents' overview

The objectives of this chapter are to analyse some new electric drive design requirements raised by dynamic driving cycles of AFVs; to introduce some novel ideas about integration modeling from the energy storage system (ESS) to motor and power electronic device design for ESS lifetime extension and to delineate a few latest control strategies of AFV traction motors related to sensorless drives and flux weakening control. The rest of this chapter is organized as follows. Section 2 describes the basic concepts of structure and main components of electric drives in AFVs. Integration of modeling and novel design of the DC active power filter for ESS lifetime extension are given in section 3. In section 4, advanced motor control strategies with respect to sensorless drives and flux-weakening regions are explained. Finally conclusions of this chapter are drawn in section 5.

2. Configurations and components of electric drives in AFVs

2.1. Electric drive configurations in various powertrains

2.1.1. Electric drives for pure electric powertrain with battery, ultracapacitor, or Hybrid Energy Storage System (HESS)

During the AFV running, the load profile consists of high current peaks and steep valleys due to the repetitive starting, acceleration, and braking in the urban driving cycle. Thus, the battery alone faces several challenges: 1) huge addition to the battery numbers to meet the peak power demand; 2) severe adverse effect on battery life because of frequent charge or discharge operations; 3) extra difficulty on battery thermal management in high-power-load situation [5].

The ultracapacitor has much higher power density, longer cycle life, lower temperature sensitivity, higher efficiencies, but lower energy density, which makes it an attractive pairing for batteries [6], [7].
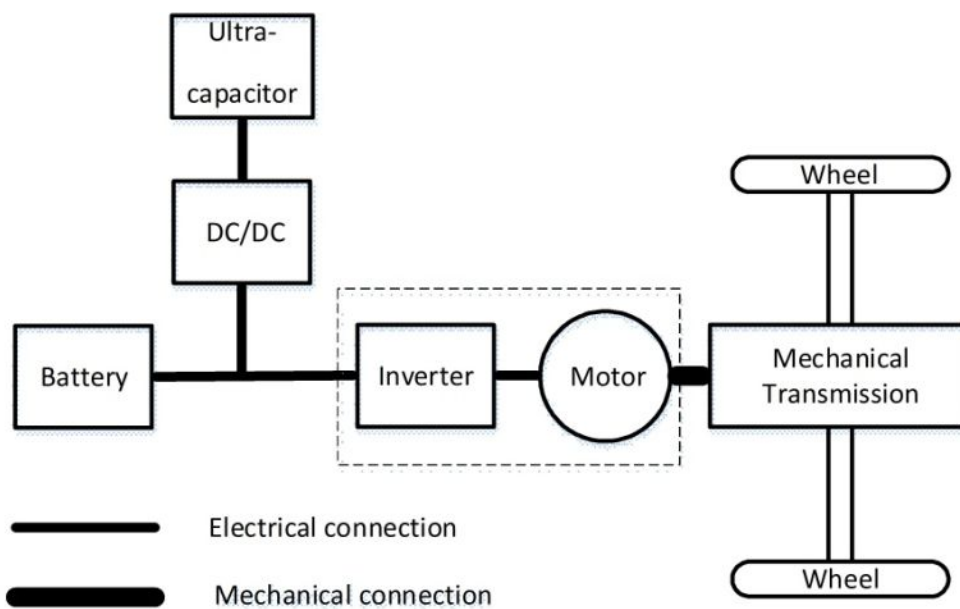

Figure 1. The configuration of hybrid energy storage system(HESS)-based electric vehicle

The topology of hybrid energy storage system is shown in Figure 1. Ultracapacitor and DC/DC converter are in series connection, with battery parallelly connected to the DC bus [8].

Hori [9], [10] adopted a heuristic control approach based on vehicle speed by taking into account ultracapacitors' energy utilization efficiency. Wang and Deng, et al. [8] adopted an optimization method for power distribution with the objective of minimum battery energy loss as the optimization goal. Ortuzar and Moreno [11] adopted heuristic algorithm based on two main rules and optimized algorithm obtained from a neural network as the energy management algorithms, respectively.

2.1.2. Electric drives for extended-range/hybrid electric powertrain with participation of engines

In a series HEV (SHEV), the internal combustion engine (ICE) is the main power source that converts the original energy in gasoline to mechanical power. The electric motor is actuated by the electricity generated by the generator or electricity stored in the battery, or both. The vehicle speed does not affect the engine speed because the engine and the wheels are decoupled. Thus, the engine can operate at its optimum speed to achieve the best fuel economy and be placed more flexibly.

A parallel hybrid electric vehicle (PHEV) adds a mechanical link (such as a clutch, belts, pulleys, and gears) between the engine and the final drive, so the engine can drive the wheels directly. The mechanical coupling adjusts the torque from the engine and the motor depending on the operation mode. The parallel hybrid electric vehicle has two propulsion devices, which can be used in motor-alone mode, combined power mode, engine-alone mode, power split mode, stationary charging mode, regenerative braking mode.

The series–parallel HEV can be operated as a series or parallel HEV. In comparison to a series HEV, the engine is coupled to the final drive through a mechanism, so the engine can deliver power to the final drive directly. In comparison to a parallel HEV, the extra mechanical output of the engine can be converted to electricity directly using the generator. The more complicated configuration brings out more flexible control strategy, better optimization of fuel economy and driveability, as well as higher cost.

2.1.3. Fuel cell vehicle based electric drives

The fuel cell powered hybrid drive train [12], [13] mainly contains a fuel cell system, a proton power system (PPS), an electric motor and accordingly motor control unit (MCU), a vehicle control unit (VCU), and a power converter between the fuel cell stack and the proton power system. After the accelerator, the braking pedal or other operating signals provide the power or torque command, the motor output power or torque is controlled by the VCU, as well as the energy flows between the fuel cell stack, the proton power system, and the drive train.

2.2. Motors, power converters, and electronic controllers of electric drives in AFVs

2.2.1. Types and brief descriptions of traction motors

Among different types of electric drives, there are four major types of motors that are viable for EVs: DC motors, induction motors, switched reluctance motor, and permanent magnet brushless motor. They possess fundamentally different machine topologies. Basically, they are classified into two main groups, the brushed and the brushless, and each group can be further classified into different subgroups.

2.2.1.1. DC motor

DC Motors are widely applied in EVs, because of the orthogonal disposition of field and armature. Simple control is the advantage of DC Motors. The permanent magnet DC Motors

allow a significant reduction due to the efficient use of radial space. Due to the low permeability of the permanent magnet DC Motors, armature reaction decreases under normal circumstances, the commutation has been greatly improved. However, their commutator and brushes make operation not very reliable and maintenance is difficult.

2.2.1.2. Induction motor

Induction motors as a brushless drive are widely used for electric vehicles, because of their low cost, high reliability, and easy maintenance. However, the induction motor performance is quite limited, such as the variable voltage variable frequency (VVVF) control. The main reason is due to the dynamic model of the nonlinearities. Recently, the induction motor has seen a greater progress in the design method, and the power density is increased. On the other hand, efficiency-optimizing-control (EOC) approaches have been developed for the EV induction drives, which can reduce the consumed energy and increase the regenerative energy. Moreover, the program of changing the pole pair number has been developed to significantly extend the constant power region.

2.2.1.3. Switched Reluctance Motor (SRM)

SRMs with simple structure have been recognized as potential traction motors for EVs [14], low manufacturing cost, and outstanding torque speed characteristics. However, design and control are difficult and, in addition, acoustic-noise is still a problem. Now, fuzzy sliding mode control has been developed for the control of nonlinear systems and minimization of chattering. In addition, vibration cancellation technique for the SRM has been proposed to reduce the vibration mode and acoustic noise.

2.2.1.4. Permanent Magnet Brushless Motor (PMBLM)

Permanent magnet brushless motors (PMBLMs) are becoming increasingly attractive and can directly compete with the induction drives for EVs. The permanent magnet synchronous motor (PMSM) and brushless DC motor (BLDCM) are two main representatives. The advantages of PMBLMs are high efficiency, high power density, and high reliability. The key problem is the high cost due to PM materials. In recent years, the new class of PMBLMs has applied hybrid field excitations.

2.2.2. Topologies of power converters and switching devices for AFVs' deployment

An integral part of the electric vehicle comprises DC-AC inverters and DC-DC converters, used as an application for EV and HEV motor drives.

2.2.2.1. DC-DC converter

Owing to the advent of intelligent vehicle systems, the demand of DC power for automotive electronic equipment is continuously increasing. A DC-DC converter possesses the function of converting the input DC voltage to another output DC voltage with different levels. A high conversion efficiency can be usually guaranteed [15]. Normally, DC-DC converters are

switching regulators with operations at high frequency. MOSFETs and IGBTs are used as switches. The size of the MOSFETs or IGBTs is drastically reduced at high-frequency operation. The switches are turned ON and OFF by pulse-width modulation (PWM) technique.

The applications of DC-DC converters have been implemented in AFVs. Bidirectional DC-DC converters are applied for battery charging, regenerative braking, and backup power. Unidirectional DC-DC converters are also used in DC motor drives and electric traction.

A bidirectional DC-DC converter as seen in Figure 2 can be divided into three main blocks. The primary side (low-voltage side) usually consists of a buck or boost-type converter and the secondary side is usually half or full-bridge arrangement.
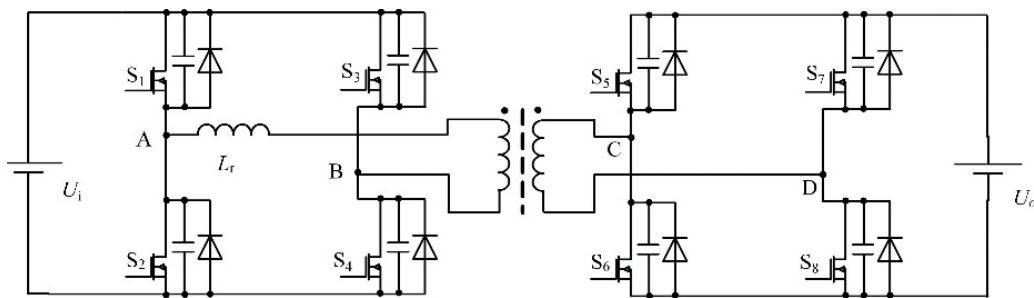

Figure 2. Full-bridge bidirectional DC-DC converter

2.2.2.2. Inverter

The DC–AC converter (inverter) has been the main choice in power electronics, because of its circuit simplicity and rugged control scheme. In order to expand the motor speed and torque region, usually high modulated frequency and high output current are permitted for the motor controlled by the inverter for AFV applications. Inverters improve the voltage utilization, reduce current harmonic contents, and create modulated sinusoidal voltage by sinusoidal PWM (SPWM) or space vector PWM (SVPWM) control methods. Three-phase two-level inverter, known as six switches inverter, shown in Figure 3, is widely used. This topology has the merits of low cost, easy control, and high reliability.
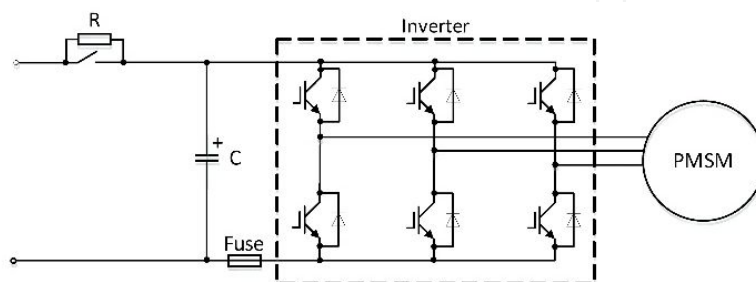

Figure 3. A common inverter topology

2.2.2.3. Soft-switching technology

Converters can be classified into two main categories: hard-switched and soft-switched for DC-DC converters and inverters. Soft-switching is a technology in which zero-voltage switching (ZVS) and/or zero-current switching (ZCS) of the switches are achieved mostly using the parasitic and/or additional components. Soft-switching reduces switching stresses (high voltage and current peaks) on the power devices during the turn-on and turn-off transients, which results in oversizing the safe operating area (SOA). Switching losses decrease for overlap size reduction of voltage and current. Severe *di/dt* and *dv/dt*, which produce electromagnetic interference (EMI), are also limited effectively [16].

2.2.2.4. Switching device

For the driving system, the high-power converter module is used. Converters control the high electric power. Insulated gate bipolar transistors (IGBTs) are used in the high-power modules as the switching devices. Other power electronics modules control the middle and low power, in which metal-oxide-semiconductor field effect transistors (MOSFETs) are used as the switching devices. The majority of devices used in power electronics are enhancement transistors, respectively, n-channel-enhancement power MOSFETs and IGBTs [17].

The main problem of the high-power modules is high electric power loss, which requires the liquid cooling system. For the future, power switching devices, very low on-resistance, and high-temperature operation are expected to simplify the cooling system of the converter. Silicon Carbide (SiC) or Gallium Nitride (GaN) devices are possible candidates. For the middle- and low-power modules, lower breakdown voltage is required. For these applications, high-frequency operation is expected, which leads to small capacitors and reactors.

2.2.3. Functions and design key points of Motor Control Units (MCUs)

1. The motor control unit (MCU) has main components:**Electronic controller**

The electronic controller consists of hardware circuit and control software. The hardware circuit mainly contains microprocessor and its minimum system, the detection circuit of motor current, voltage, speed, temperature, all kinds of hardware protection circuit, and the communication circuit (CAN Bus) with the external control unit like the vehicle controller and battery management system to exchange data. The control software realizes corresponding control algorithm depending on different types of motors. For instance, the strategies of flux weakening control, $i_d=0$ control and MTPA control are widely used in PMSM control software.

2. **Driver**

It converts the motor control signal which comes from microcontroller to PWM signal, which drives the power converter and implements the isolation of power signal and control signal.

3. **Power converter**

The power converter controls the motor current. The power devices that are widely used in electric vehicles contain the gate-turn-off thyristor (GTO), MOSFET, IGBT, and smart power module, etc.

During the development process, several key technologies have to be analyzed, such as the design of power circuits, heat sink, and the control strategies development as well as kinds of hardware and software protection functions.

3. New definitions of modeling and design of the DC APF for electric drives in AFVs

3.1. New definitions of mathematical modeling integration from ESS to motor

3.1.1. Purposes and meanings of multidomain coupling unified mathematical expressions for electric drives

In the past decade, plenty of literature has focused on the operation performance, parameter optimization, and control strategies of components in AFV electric drives. These researchers mostly use DC power supplies or electronic loads to simulate input/output characteristics of components, and meanwhile realistic influence between components (e.g., battery and traction motor) is seldom considered. To the author's best knowledge, there are no publications that regard the electric drive system as a whole for the systematic research on multidomain (dynamics, electromagnetics, electrochemistry, etc.) coupling mechanism.

The electric motors are required to operate in complicated conditions of frequent start/stop and acceleration/deceleration. High torque is needed at low speeds or when running uphill, while low torque is needed at high speeds. In the meantime, speed adjusting range should be very wide. This is significantly different from the industry applications where usually rated conditions are assigned to the electric motors. Therefore, the transient performance require-ments for the AFV electric motors are very high and, further, are transferred to high transient requirements on the ESS through three-phase inverter. Additionally, the switching frequency of switching devices (e.g., IGBT) is high up to several or tens of kHz, the switching commu-tation time is extremely short, and the disturbance currents including diode recovery current exist, so the uncertain high-frequency transient chaotic currents should be produced across the ESS. The phenomenon will do harm to the stability and even lifetime of the ESS. Detailed descriptions can be found in section 3.2.1.

On the other hand, the ESS (battery for specific) AC impedance (including ohmic resistance, polarization resistance, capacitive reactance, Warburg impedance, and so on) characteristics will have impact on the transient performance of traction motors. The AC impedance charac-teristics of the battery determine the battery output power capability (supposing the electro-chemical potential is a constant) and further influence the transient output power capability of the traction motor via the inverter. Consequently, the motor transient performance could be somehow restricted.

Thus, this section is aimed at importing new definitions of electric drive unified mathematical expressions for systematic exploration of transient multidomain coupling mechanism from dynamics-electromagnetics-electrochemistry based on the ESS, traction motor, inverter, and

DC-DC converter in the AFV electric drive system. Multiple subjects could be melted including energy storage, electric machine, and power electronics. The entire electric drive can be regarded as a whole without separating relationships between components, and a unified and general mathematic expression is capable of identifying specific numeric relations between transient requirements and parameters of components. In addition, the systematic-, circuit-, and component-class parameter optimization aimed at efficiency improvement in electric drives of alternative fuel vehicles could be achieved.
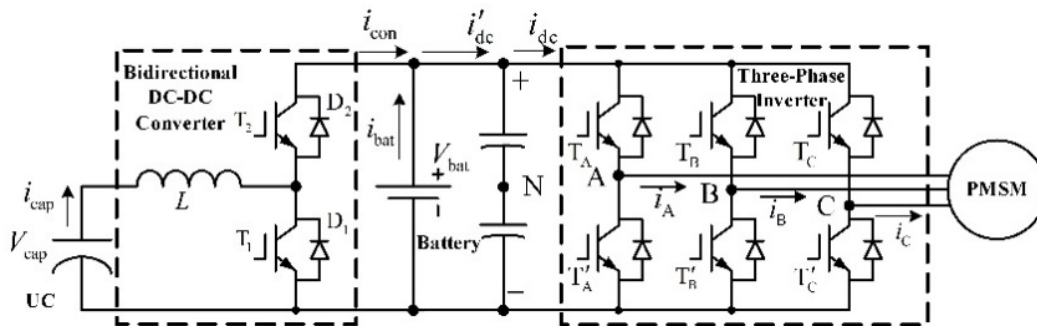
3.1.2. Modeling framework delineation

Figure 4. Circuit topology of the electric drive system

Considering comprehensiveness, an ESS including a battery and ultracapacitor is studied. The electric drive with only the battery is analyzed similarly and more easily. The circuit topology of the studied electric drive system in AFV is shown in Figure 4. The EV traction motor is a permanent magnet synchronous motor (PMSM) and the three-phase inverter is comprised of six IGBTs. The UC and battery are connected to the low-voltage (LV) and high-voltage (HV) sides respectively of the bidirectional DC-DC converter, which is constructed in a half-bridge topology.

Individual transient mathematical models (including the PMSM, inverter, DC-DC converter, ultracapacitor, and lithium-ion battery) of all components are built first. For instance, the switching state function is introduced to set up a nonlinear model of the inverter and then it is transferred to a linear model with help of the large-signal disturbance method. The lithium-ion battery is modeled using the scheme combining with the equivalent circuit and electro-chemical factor-assisted electrical parameter adaptive-adjusting.

The speed ω and torque T of the traction motor are chosen as unified inputs for the integrated systematic model. The individual model is transformed into expressions by $\omega(t)$ and $T(t)$. Thus, the multidomain models are related to each other using the unified inputs.

The important variables in all individual models can be finally expressed by $\omega(s)$ and $T(s)$, where s is a Laplace operator. The time-domain mathematical descriptions for these variables could also be acquired using combination of inverse Laplace transformation and some additional mathematical methods (e.g., residues method). Therefore, the multidomain

coupling transient model for the AFV electric drives can be derived and complete frequency- and time-domain expressions of all variables as well.

3.2. Design of DC active power filter for ESS chaotic current elimination

3.2.1. Exploration of Interior relationship between traction motor output performance and ESS current ripples

The output A-phase voltage of the inverter can be expressed as its Fourier series expansions, as follows:

$$V_{AN} = \sum_{k=0}^{+\infty} V_k \sin(k\omega t) \tag{1}$$

where V_k denotes the component of order k, ω represents the fundamental angular frequency. We can define $\alpha = 2\pi/3$ as the angular difference between two of three phases.

Regardless of the unbalanced currents problem, the nonsinusoidal phase currents can be depicted as follows:

$$i_A = \sum_{m=0}^{+\infty} I_m \sin(m\omega t + \varphi_m), i_B = \sum_{m=0}^{+\infty} I_m \sin(m(\omega t - \alpha) + \varphi_m), i_C = \sum_{m=0}^{+\infty} I_m \sin(m(\omega t + \alpha) + \varphi_m) \tag{2}$$

The DC bus current can be considered as sum of currents through three bridges in the inverter. Meanwhile, one bridge's contribution is composed of the currents from upper and lower branches. Consequently, the DC bus current is obtained as:

$$i_{dc} = i_{dc,A,1} + i_{dc,A,2} + i_{dc,B,1} + i_{dc,B,2} + i_{dc,C,1} + i_{dc,C,2} \tag{3}$$

where the subscript 1 represents the upper branch, and 2 represents the lower branch.

As an instance, the upper and lower currents for the Phase-A bridge are described as:

$$i_{dc,A,1} = K_{A,1} i_A, i_{dc,A,2} = K_{A,2} i_A \tag{4}$$

where the coefficients are $K_{A,1} = \dfrac{V_{AN}}{V_{bat}} + \dfrac{1}{2}$, and $K_{A,2} = \dfrac{V_{AN}}{V_{bat}} - \dfrac{1}{2}$. The Phase-B and Phase-C currents can be computed similarly. With expressions given by equations (1)-(4), the upper and lower currents of three bridges are available to be calculated.

Substituting equation (4) and similar expressions for the other two phases into (3), the DC bus current can be obtained in the form of Fourier series as:

$$i_{dc} = \sum_{m=1}^{+\infty} \frac{2I_m}{V_{bat}} \left\{ \sum_{k=1}^{+\infty} \frac{V_k}{2} \cos((k-m)\omega t - \varphi_m) \times [2\cos(k-m)+1] \right.$$
$$\left. + \sum_{k=1}^{+\infty} \frac{V_k}{2} \cos((k+m)\omega t + \varphi_m) \times [2\cos(k+m)+1] \right\}$$

(5)

Finally, after combining similar terms and sequent calculation, the DC bus current expression is simplified to:

$$i_{dc} = \sum_{m=1}^{+\infty} \frac{3I_m}{V_{bat}} \sum_{k=1}^{+\infty} (V_{3k+m} - V_{3k-m}) \cos(3k\omega t - \varphi_m)$$

(6)

3.2.2. Overall descriptions for the novel DC active power filter

The operation principle of the proposed DC active power filter (APF) is delineated in Figure 5. The motor controller calculates the synchronous electrical angle and synchronous frequency of phase currents after acquiring rotor position and current/voltage signals. Thus, the fundamental frequency and the fundamental phase for the Fourier Transform of the DC bus current are determined with respect to the theoretical analysis in section 3.2.1. It has to be noted that every Fourier Transform decomposition period could give its information to the current allocation of the next period. So it is available to be predicted that the resulted low-frequency components (closely related to the PMSM speed) cannot change in such a short time. The high-frequency components are derived from the difference of the real-time samplings of the DC bus current and low-frequency components calculated in the previous processing period.
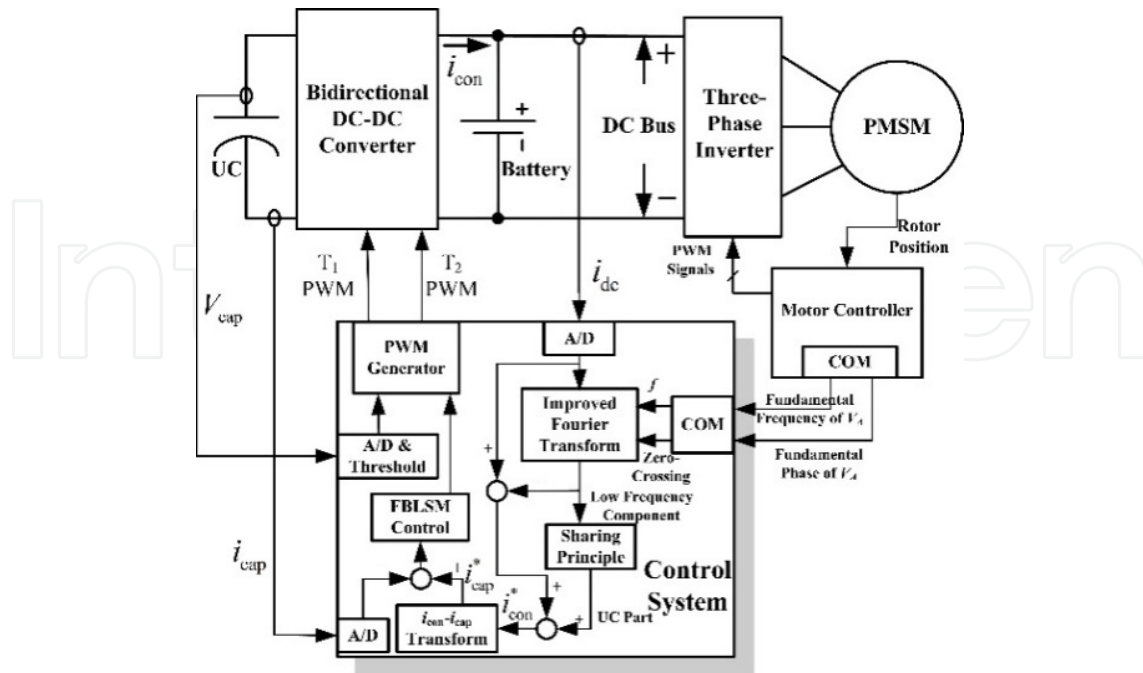

Figure 5. Operation principle of the proposed APF strategy with help of motor information.

In the peak power demand process (e.g., acceleration, uphill), the UC is commanded as a large power provider. Thus, the low-frequency components from the DC bus current should be shared reasonably by the UC and battery considering their respective power density. In this paper, the current directly from the UC is considered as a control variable; thereafter, the output current reference i_{con}^{*} on the DC-DC converter high-voltage side has to be transformed to the counterpart i_{cap}^{*} on the low-voltage side, complying with the power conservation law and estimated efficiency. The fixed-boundary-layer sliding mode (FBLSM) control is applied to achieve pulse-width-modulation (PWM) duty cycle for one of two IGBTs (choose T1 or T2 regarding power flow direction) due to consideration of eliminating of control chattering usually caused by frequent control switching in normal sliding mode control. In the meantime, the UC discharging stops when UC SOC reaches the desired lower limit, and then the battery or regenerative braking UC immediately helps UC increase its SOC to a preset value for the further use.

3.2.3. Improved fast fourier transform for frequency components' decomposition of ESS currents

The Discrete Fourier Transform (DFT) and Inverse Discrete Fourier Transform (IDFT) are expressed as the following two equations, respectively:

$$X\left(k\right)=\sum_{n=0}^{N-1}x\left(n\right)e^{-j\frac{2\pi kn}{N}}=\sum_{n=0}^{N-1}x\left(n\right)W_{N}^{kn}, \quad 0\leq k \leq N-1 \tag{7}$$

$$x\left(n\right)=\frac{1}{N}\sum_{k=0}^{N-1}X\left(k\right)e^{j\frac{2\pi kn}{N}}=\sum_{k=0}^{N-1}x\left(k\right)W_{N}^{-kn}, \quad 0\leq n \leq N-1 \tag{8}$$

In order to speed up the computation, the normal FFT is used. The FFT calculation is finally transformed to only two computations by using the following expressions:

$$X\left(k\right)=G(k)+W_{N}^{k}H(k), \quad 0\leq k \leq \frac{N}{2}-1 \tag{9}$$

$$X\left(k+\frac{N}{2}\right)=G(k)-W_{N}^{k}H(k), \quad 0\leq k \leq \frac{N}{2}-1 \tag{10}$$

where $G(k)=\sum_{r=0}^{N/2-1}x(2r)W_{N/2}^{rk}$ and $H(k)=\sum_{r=0}^{N/2-1}x(2r+1)W_{N/2}^{rk}$

To minimize the side lobes, the Blackman-Harris Window as a generalization of the Hamming family, is given by:

$$w\left(n\right)=\sum_{k=0}^{3}(-1)^{k}a_{k}\cos\left(\frac{2\pi kn}{N}\right) \tag{11}$$

Therefore, the improved FFT expression with the Blackman-Harris Window can be shown as follows based on equations (9) and (10):

$$X_w(k) = \sum_{i=0}^{3} (-1)^i \frac{a_i}{2} \left[X(k-i) + X(k+i) \right] \tag{12}$$

With use of the improved FFT, the high-frequency and low-frequency components can be decomposed from the load demand, for the power distribution to UC and battery, as shown in Figure 5.

4. Advanced motor control strategies for AFV-based electric drives

4.1. Overview of traction motor speed/torque control strategies

4.1.1. Speed/torque vector control

The concept of vector control was first proposed by Siemens' F. Blaschke in the early 1970s, which is also named as field-oriented control (FOC). In this method, the stator current of a three-phase AC motor is transformed into two orthogonal components [18]. One component can control the magnetic flux; the other can control the torque.

In a typical FOC block diagram for a permanent magnet synchronous motor (PMSM), the control system first transforms the command speed or torque into the corresponding current command i_d^*, i_q^*. Then, proportional-integral (PI) controllers are used as current regulator to generate the reference d–q axis reference voltage. The transistor switching is defined by the pulse-width modulation signal according to the stator references voltage.

For the FOC system, the most important thing is to realize the Clarke and Park transformation. It is these transformations that connect the three-phase coordinate system to the $d-q$ axis coordinate system. The Clarke transformation converts three-phase currents to a two-axis plot to create time-varying quadrature-current values i_α and i_β. And the Park transformation is between the stationary coordinates $\alpha-\beta$ and the $d-q$ coordinate reference frame rotated to align with the rotor flux. As the d axis is always in the direction of magnet flux linkage and q axis in the quadrature direction, the values of i_d and i_q remain constant. The flux and torque are separately controlled by stator direct-axis current i_d and quadrature-axis current i_q.

FOC is used to control the AC synchronous and induction motors by transforming their dynamic structure into that of DC machines. Unfortunately, the scheme requires many electronic components such as sensors, amplifiers, or multipliers which increase the cost and more calculations are needed to realize the control strategy. This situation is changed due to the availability of microelectronics, with the cost of control hardware being no longer a major consideration [19].

4.1.2. Direct Torque Control (DTC)

Direct torque control (DTC) is a method that controls the torque (and thus finally the speed) of three-phase AC electric motors. The key point of this control is to select stator voltage vectors according to the differences between the references of torque and stator flux linkage and their actual values estimated on basis of the measured voltage and current of the motor [20], [21].

In a PMSM drive with DTC, the dq axis currents i_d and i_q, are obtained from the measured three-phase currents, and the voltages v_d and v_q are calculated from the dc-link voltage, since the voltage vectors determined by the switching table are known. By integrating the stator voltages, we can calculate the stator flux linkage. Torque is calculated by a cross product of calculated stator flux linkage vector and measured motor current vector. Then the calculated flux magnitude and torque are compared with their reference values to get the flux and torque errors. If either the calculated flux or torque deviates from the reference more than the allowed tolerance, the transistors of the variable frequency drive are turned off and on to generate one certain voltage.

Without the current controller followed by a pulse-width modulation (PWM) comparator, and not using the parameters of the motor, except the stator resistance, the DTC owns the advantages of less parameter dependence and fast torque response when compared with the torque control via PWM current control. But torque and flux linkage ripples are always the main disadvantage of the DTC.

4.2. Sensorless drives for Permanent Magnet Synchronous Motors (PMSMs) in AFVs

Due to the characteristic of getting rid of sensors and reduction of cost and systematic complexity, the sensorless drives for AFV motors have attracted great interest of the auto industry. In a sensorless drive, the motor speed could be accurately estimated through some sophisticated observer and some other electrical parameters (currents, voltages, or flux) as well. Sliding mode control has been widely used for motor control systems because of its insensitive characteristics to disturbances of motor parameters. With the same property, sliding mode observers (SMOs) have been adopted by researchers and the industry in the last decade applied to the motor drives for precise estimation of speed and flux. It is more robust to the operating conditions and systematic uncertainties. However, it has to be noted that imperfect implementation of the switching leads to chattering, which is a major drawback of SMO. Thus the following section will introduce a new fixed-boundary-layer sliding mode observer for AFV motor drives, considering reduction of chattering and guaranteeing estimation precision in a wide speed range.

4.2.1. Mathematical model of studied motor

The induction motor is studied as an example for the explanation of the proposed sliding mode observer. Its mathematical model could be described in the rotating d-q frame [22] as follows.

Let i_d and i_q, V_d and V_q, ω_r, T_L, ψ_{rd}, θ, , p, and J stand for stator currents, stator voltages, rotor speed, load torque, direct-axis rotor flux, flux angle, pole pair number, and moment of inertia.

$\tau_r = L_r / R_r$ represents the rotor time constant, and $\sigma = 1 - L_m^2 / L_s L_r$ is the leakage magnetic coefficient. For analysis simplicity, set $m = (L_r R_s + L_m^2 R_r) / (\sigma L_s L_r^2)$, $\gamma = L_m / (\sigma L_s L_r)$, $\varsigma = 1 / (\sigma L_s)$, $\kappa = 1 / \tau_r$, $\rho = p L_m / L_r$, and the motor model can be written below:

$$
\begin{cases}
\dfrac{\mathrm{d}i_d}{\mathrm{d}t} = -m i_d + \kappa \gamma \psi_{rd} + p \omega_r i_q + \kappa \dfrac{L_m}{\psi_{rd}} i_q^2 + \varsigma V_d \\[2mm]
\dfrac{\mathrm{d}i_q}{\mathrm{d}t} = -m i_q - \gamma p \omega_r \psi_{rd} - p \omega_r i_d - \kappa \dfrac{L_m}{\psi_{rd}} i_d i_q + \varsigma V_q \\[2mm]
\dfrac{\mathrm{d}\theta}{\mathrm{d}t} = p \omega_r + \kappa \dfrac{L_m}{\psi_{rd}} i_q \\[2mm]
\dfrac{\mathrm{d}\psi_{rd}}{\mathrm{d}t} = -\kappa \psi_{rd} + \kappa L_m i_d \\[2mm]
\dfrac{\mathrm{d}\omega_r}{\mathrm{d}t} = \rho \psi_{rd} i_q - \dfrac{1}{J} T_L
\end{cases}
\tag{13}
$$

4.2.2. Design of fixed-boundary-layer sliding mode observer

In this study, the three-phase stator currents are the only required measures, and these are transformed from the three-phase reference frame to a diphasic reference frame, and then to the frame of the rotating field (d-q) as follows:

$$
\begin{cases}
i_d = \sqrt{\dfrac{2}{3}} \left(\cos(\hat{\theta}) i_a + \cos(\hat{\theta} - \dfrac{2}{3}\pi) i_b + \cos(\hat{\theta} + \dfrac{2}{3}\pi) i_c \right) \\[3mm]
i_q = \sqrt{\dfrac{2}{3}} \left(-\sin(\hat{\theta}) i_a - \sin(\hat{\theta} - \dfrac{2}{3}\pi) i_b - \sin(\hat{\theta} + \dfrac{2}{3}\pi) i_c \right)
\end{cases}
\tag{14}
$$

where i_a, i_b, and i_c represent the three-phase stator currents, respectively, and $\hat{\theta}$ denotes the estimated flux angle. Relation between the estimated flux angle and rotor speed could be derived from system (13) as follows:

$$
\frac{\mathrm{d}\hat{\theta}}{\mathrm{d}t} = p \hat{\omega}_r + \kappa \frac{L_m}{\hat{\psi}_{rd}} i_q
\tag{15}
$$

Assume that system (13) has the outputs $(y_1 \quad y_2)^T = (i_d \quad i_q)^T$. Unfortunately, it could be found that ψ_{rd} in system (13) is not observable. Reference [24] has proved that system (13) has a stable zero dynamics about ψ_{rd} with the output $y_1 = i_d$ and $\kappa > 0$. Thus, it is possible to estimate ψ_{rd} by designing an estimator, and then ω_r becomes observable. The sliding mode observer technology is employed to estimate ω_r. The required voltage d-q frame in the observer is obtained from outputs of voltage feedforward compensation part. The description of the fixed-boundary-layer sliding mode (FLBSM) observer is given below.

$$\begin{cases} \dfrac{d\hat{i}_d}{dt} = -mi_d + B_1\kappa\gamma\hat{\psi}_{rd} + B_1\lambda_1(i_d - \hat{i}_d) + B_1\kappa\dfrac{L_m}{\psi_{rd}}i_q^2 + \varsigma V_d \\[3mm] \dfrac{d\hat{\psi}_{rd}}{dt} = -\kappa\hat{\psi}_{rd} + \kappa L_m i_d \\[3mm] \dfrac{d\hat{\omega}_r}{dt} = B_1\rho\hat{\psi}_{rd}i_q + B_2\lambda_2\mathrm{sat}((\tilde{\omega}_r - \hat{\omega}_r),\phi_1) \\[3mm] \hat{T}_L = -B_3 J\lambda_2\mathrm{sat}((\tilde{\omega}_r - \hat{\omega}_r),\phi_1) \end{cases} \tag{16}$$

where $\tilde{\omega}_r = \dfrac{B_2\lambda_1\mathrm{sat}((i_d - \hat{i}_d),\phi_2)}{pi_q}$ denotes the auxiliary state of the rotor speed positioned where the speed measurement originally stays for observer design, $\hat{i}_d$ is an intermediate variable required by the observer to obtain estimation of other parameters so that i_d could be measured, and the function sat(x, ϕ) is defined below:

$$\mathrm{sat}(x,\phi) = \begin{cases} x/\phi & \text{if } |x| < \phi \\ \mathrm{sgn}(x) & \text{otherwise} \end{cases} \tag{17}$$

The coefficients B_1, B_2, and B_3 in observer (16) are depicted as follows:

$$B_1 = \begin{cases} 0, & \text{if } |\hat{\psi}_{rd} - \psi_{rd}| > \varepsilon \\ 1, & \text{otherwise} \end{cases} \tag{18}$$

$$B_2 = \begin{cases} 0, & \text{if } \hat{i}_d \neq i_d \\ 1, & \text{otherwise} \end{cases} \tag{19}$$

$$B_3 = \begin{cases} 0, & \text{if } \hat{\omega}_r \neq \tilde{\omega}_r \\ 1, & \text{otherwise} \end{cases} \tag{20}$$

Then, the theorem that the sliding mode observer can exponentially converge will be proved. Assume that the observation error of ψ_{rd}, $e_1 = \psi_{rd} - \hat{\psi}_{rd}$, exceeds ε (i.e., $B_1 = 0$), and $de_1/dt = -\kappa e_1$ where $\kappa > 0$ can be obtained. A Lyapunov function $V_{e_1} = 0.5e_1^2$ is designed. Then $dV_{e_1}/dt = -\kappa e_1^2 < -\kappa\varepsilon^2 < 0$ can be obtained. The exponential convergence of $\hat{\psi}_{rd}$ to ψ_{rd} is proved. Therefore, a certain instant t_1 can always be found such that when $t > t_1$, we have $e_1 \leq \varepsilon$ given a sufficiently small real $\varepsilon > 0$. At this moment, $B_1 = 1$. Next $e_2 = i_d - \hat{i}_d$ is defined. When $t > t_1$, the following equation can be derived as:

$$\frac{\mathrm{d}e_2}{\mathrm{d}t} = p\omega_r i_q + \left(\kappa\gamma - \frac{\kappa L_m i_q^2}{\psi_{rd}\hat{\psi}_{rd}}\right)e_1 - \lambda_1 \mathrm{sat}(e_2, \phi_2) \tag{21}$$

To prove the convergence of $\hat{i}_d$ to i_d, a Lyapunov function $V_{e_2} = \frac{1}{2}e_2^2$ is used. We set

$$\lambda_1 = \max\left\{\left(\kappa\gamma - \frac{\kappa L_m i_q^2}{\psi_{rd}\hat{\psi}_{rd}}\right)e_1 + p\omega_r i_q\right\} + \xi_2 \tag{22}$$

and the differential of the Lyapunov function can be delineated as:

$$\frac{\mathrm{d}V_{e_2}}{\mathrm{d}t} = \left(\left(\kappa\gamma - \frac{\kappa L_m i_q^2}{\psi_{rd}\hat{\psi}_{rd}}\right)e_1 + p\omega_r i_q - \lambda_1 \mathrm{sat}(e_2, \phi_2)\right)e_2 \leq -\xi_2|e_2| = -\sqrt{2V_{e_2}}\,\xi_2 \tag{23}$$

Consequently, $\hat{i}_d$ converges to i_d in a finite time t_2. When $t > t_2$, $B_1 = 1$ and $\frac{\mathrm{d}e_2}{\mathrm{d}t} = e_2 = 0$ are obvious. So according to (21), the new relation establishes below:

$$p\omega_r i_q + \left(\kappa\gamma - \frac{\kappa L_m i_q^2}{\psi_{rd}\hat{\psi}_{rd}}\right)e_1 - \lambda_1 \mathrm{sat}(e_2, \phi_2) = 0 \tag{24}$$

We set $E = \left(\kappa\gamma - \frac{\kappa L_m i_q^2}{\psi_{rd}\hat{\psi}_{rd}}\right)e_1 \bigg/ pi_q$, so the auxiliary state of rotor speed is given by:

$$\tilde{\omega}_r = \omega_r + \left(\kappa\gamma - \frac{\kappa L_m i_q^2}{\psi_{rd}\hat{\psi}_{rd}}\right)e_1 / pi_q = \omega_r + E \tag{25}$$

E and $\frac{\mathrm{d}E}{\mathrm{d}t}$ exponentially converge to zero due to the convergence of the rotor flux. Thus, the fact that $\tilde{\omega}_r$ exponentially converges to ω_r is proved. Then we have:

$$\frac{\mathrm{d}\tilde{\omega}_r}{\mathrm{d}t} = \frac{\mathrm{d}\omega_r}{\mathrm{d}t} + \frac{\mathrm{d}E}{\mathrm{d}t} = \rho\psi_{rd}i_q - \frac{1}{J}T_L + \frac{\mathrm{d}E}{\mathrm{d}t} \tag{26}$$

A Lyapunov function $V_{e_3} = \frac{1}{2}e_3^2$ is used for proof of convergence of $\hat{\omega}_r$ to $\tilde{\omega}_r$ assuming $e_3 = \tilde{\omega}_r - \hat{\omega}_r$. Let

$$\lambda_2 = \max\left\{\rho i_q e_1 - \frac{1}{J}T_L + \frac{\mathrm{d}E}{\mathrm{d}t}\right\} + \xi_3 \tag{27}$$

given $\xi_3 > 0$. Then, the following equation can be obtained:

$$\frac{\mathrm{d}V_{e_3}}{\mathrm{d}t} = \left(\rho i_q e_1 - \frac{1}{J}T_L + \frac{\mathrm{d}E}{\mathrm{d}t}\right)e_3 \leq -\xi_3|e_3| = -\sqrt{2V_{e_3}}\,\xi_3 \tag{28}$$

Therefore, the convergence of $\hat{\omega}_r$ to $\tilde{\omega}_r$ in a finite time t_3 is proved. When $t > t_3$, $B_3 = 1$ and $\dfrac{\mathrm{d}e_3}{\mathrm{d}t} = e_3 = 0$ are obvious. Thus,

$$\hat{T}_L = T_L - J\rho i_q e_1 - J\frac{\mathrm{d}E}{\mathrm{d}t} \tag{29}$$

As mentioned above, both $\tilde{\omega}_r$ and $\hat{\psi}_{rd}$ exponentially converge, so e_1, E, and $\mathrm{d}E/\mathrm{d}t$ exponentially converge to zero. Therefore, the convergence of $\hat{T}_L$ to T_L is finally proved.

The reference, experimental, and estimated values of rotor speed of the electric motor are compared in Figure 6. To test the robustness of the observer, +100% resistance change is considered and the -50% load torque and +100% stator leakage inductance changes as well. We can see that the actual speed tracks the reference trajectory well using the proposed controller, and no distinct speed differences between estimation and measurement occurred. Because of small inaccuracy due to the current harmonics, differences between the estimated and measured speed at low speeds seem a little bit bigger than those at high speeds. However, the situation is also acceptable in real operation.
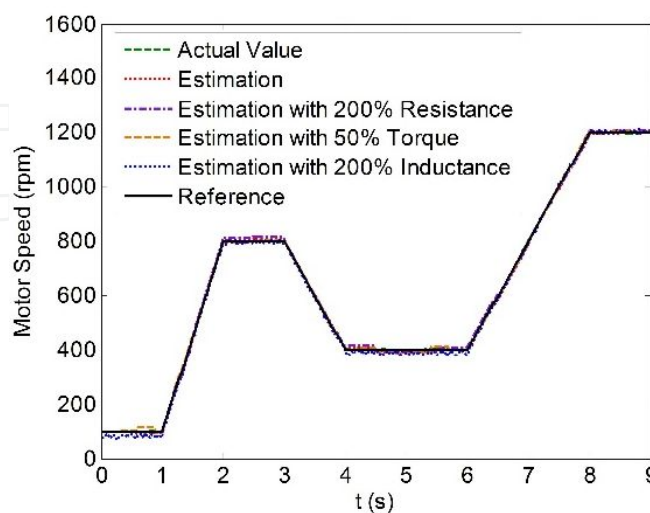

Figure 6. Comparison between references and estimated speeds using FBLSM observer

Rotor flux comparison is also studied, given the flux reference. Unlike the rotor speed results, estimated rotor flux is not precisely approaching the reference (see Figure 7), which is however close to actual results. The "actual value" shown in Figure 7 for comparison is obtained from normal flux calculation method through measured voltages and currents and could be considered as actual flux due to proof of incomputable applications. It is clear that the estimated flux with +200% resistance, 50% load torque, or +200% stator leakage inductance is not influenced by these disturbances dramatically.
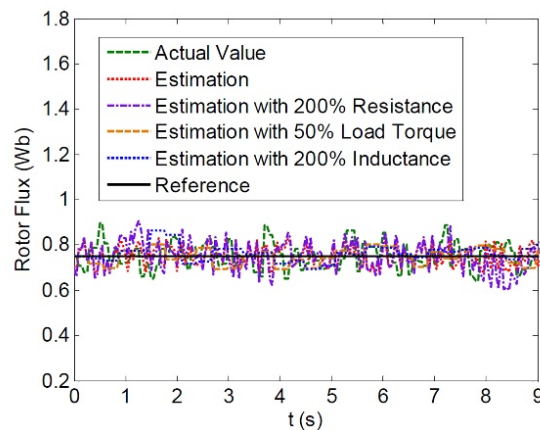

Figure 7. Comparison between references and estimated rotor flux using FBLSM observer

4.3. Advanced flux-weakening control at high speeds required by AFE driving

In AFVs, the traction motor has a very wide speed range, which needs flux-weakening control strategy to make the motor work at high speeds.

4.3.1. Classification of traction motor operation ranges

Figure 8 illustrates the characteristics of a permanent magnet synchronous motor used in AFVs. All the operation ranges can be divided into three parts: constant torque, constant power, and high-speed region. When the rated speed is not reached, the PMSM works in the constant-torque region, exerting a constant torque (rated torque). Once the speed reaches the rated motor speed, the torque begins to drop proportionally compared with speed, leading to a constant output power. The constant-power region ends when the following high-speed region starts. Then with the square of the speed, the motor torque drops proportionally [23].

4.3.2. Depictions of condition identification for flux-weakening control

Permanent magnet synchronous motors (PMSMs) fed by PWM inverters are widely used for industrial applications, especially servo drive applications, which always work in rated condition. But in traction and spindle drives, higher speed is needed [24]. When in constant-power region, the motor is always controlled by the flux-weakening control method.

In the constant torque region, the stator voltage increase as the internal EMF of the motor rises in proportion to the motor speed. However, when the speed rises to rated speed, the voltage
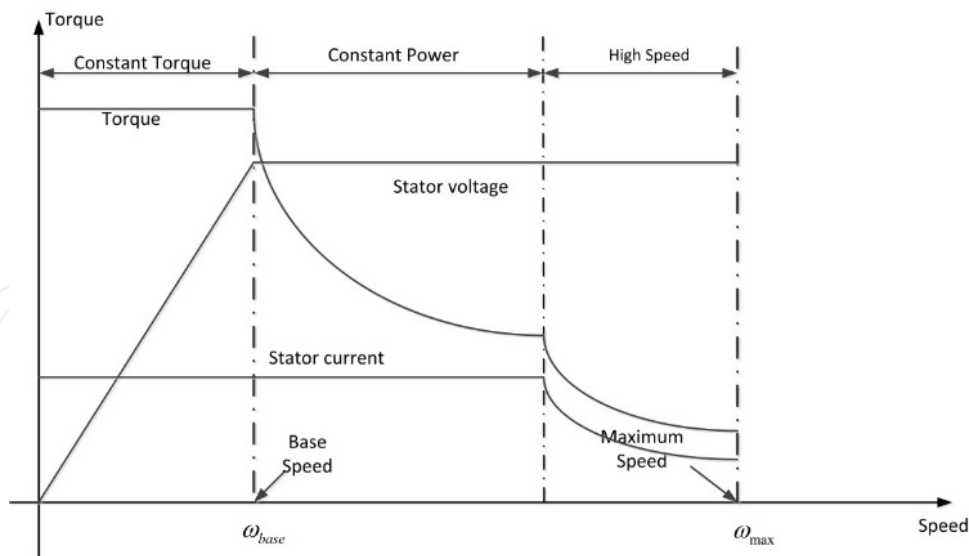
Figure 8. Characteristic curve of PMSM

limit of the associated frequency converter is reached. The internal voltage must now be adjusted to be compatible with the applied converter voltage. However, since the permanent magnets inherently provide the equivalent of a constant field excitation, the internal EMF of the machine continues to increase as speed increases. So the air gap flux should be weakened by the demagnetizing effect due to the d-axis armature reaction, which is called flux weakening [25].
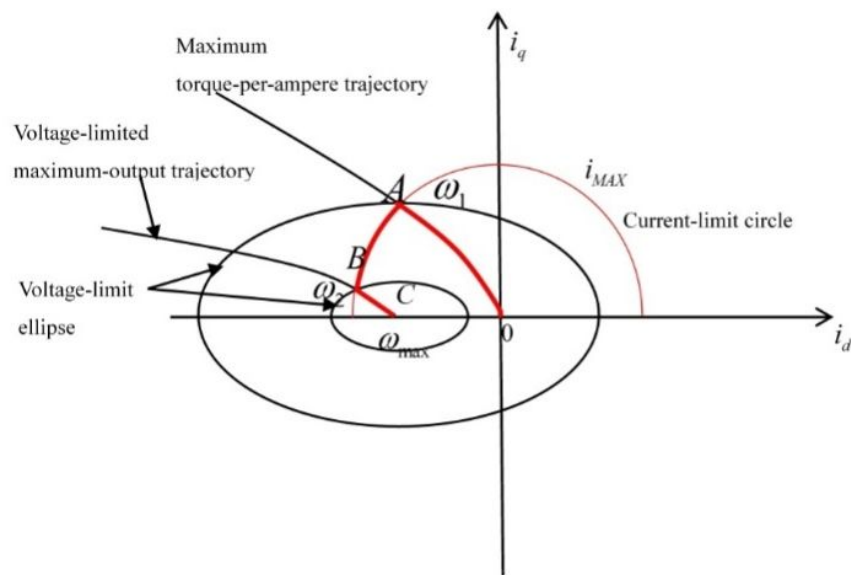

Figure 9. $i_d - i_q$ plane

On the $i_d - i_q$ plane (see Figure 9), there are a current-limit cycle and voltage-limit ellipse. These two limits are all decided by the inverter capacity. The maximum torque-per-ampere current

vector trajectory is used in the constant torque region to generate maximum torque. The voltage-limited maximum output trajectory makes the motor increase to higher speed.

Region I ($\omega \leq \omega_1$): i_d and i_q are constant values given by the maximum torque-per-ampere (MTPA) trajectory. The maximum output torque is usually achieved in point A in Figure 8, where stator current $I_s = I_{\lim}$, stator voltage $V_s < V_{\lim}$

Region II ($\omega_1 < \omega \leq \omega_2$): when the speed reaches ω_1 and stator voltage increases to maximum voltage, the current vector starts to moves from A to B along the current limit circle as the rotor speed increases. In this region, stator current $I_s = I_{\lim}$, stator voltage $V_s = V_{\lim}$

Region III ($\omega_2 < \omega$): when at point B, $\omega = \omega_2$, the current vector starts to move along the voltage-limited maximum output trajectory, where stator current $I_s < I_{\lim}$, stator voltage $V_s = V_{\lim}$ [26].

4.3.3. Proposal of novel flux-weakening control based on nonlinear current compensation

Figure 10(a) illustrates the block diagram of the novel flux-weakening control based on nonlinear current compensation. Part 1 is the torque controller in the constant torque region. The current command i_s^* is the output of the P1I speed controller, and then decomposed into d- and q-axes components, i_{dx}^* and i_{qx}^* according the maximum torque-per-ampere trajectory until the current regulator begins to saturate.
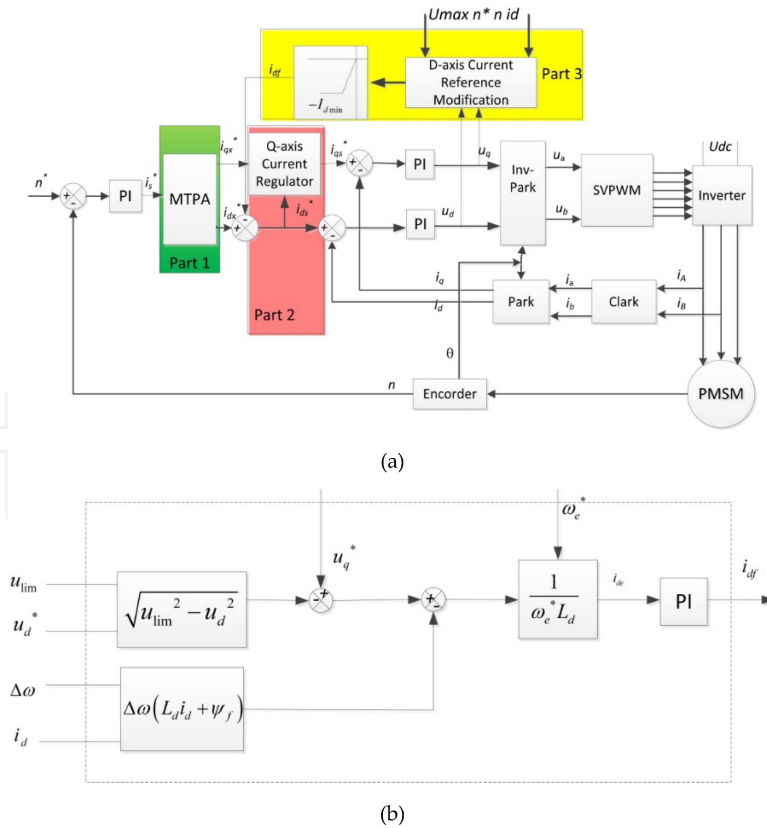

(a)

(b)

Figure 10. (a) The block diagram of the novel flux-weakening control based on nonlinear current compensation. (b) d-axis current modification

The proposed flux-weakening controller includes Parts 2 and 3. The proposed flux-weakening control algorithm uses the output reference voltage of the synchronous PI current regulator to identify the onset of the flux weakening. As the speed of the IPMSM increases, the output of the current regulator approaches to the boundary of the pulse-width modulator. With the reduced margin of the voltage, the performance of the current regulator gets worse and finally loses its controllability. As shown in Figure 10(b), the controller ensures the margin of the voltage by compensating the d-axis current toward the negative direction to prevent saturation of the current regulators. But at the low-speed region, the output voltage of the current regulator is usually less than $V_{\max}$ and thus Part 3 is not activated. The function of Part 2 is to adjust the q-axis current command $i_{qx}{}^*$, as the d-axis current command $i_{qs}{}^*$ increased toward the negative direction, because of the current limit $I_{s\max}$.

5. Conclusions

In this chapter, some fundamentals of the electric drives in alternative fuel vehicles are first introduced including application background and existing challenges. Then the multidomain transient unified modeling of AFV electric drives is newly defined at aim of efficiency improvement and ESS lifetime extension. The active power filter (APF) in the DC system is proposed for the elimination of ESS chaotic currents. The sensorless drive for the traction motor using a fixed boundary layer sliding mode observer is described in detail, as well as the flux-weakening controller using nonlinear current compensation, in order to enhance traction motor control precision and dynamic performance. The definitions and strategies discussed in this chapter may contribute to research and development of brand-new electric drives applied in EVs or HEVs.

Acknowledgements

Author details

Xi Zhang

Address all correspondence to: braver1980@sjtu.edu.cn

Institute of Automotive Engineering, Shanghai Jiao Tong University, Shanghai, China

References

[1] Paiva SLD, Savi MA, Viola FM, Leiroz AJK. Global warming description using Daisyworld model with greenhouse gases. *Biosystems*. 2014;125(2014):1-15. DOI: 10.1016/J.BIOSYSTEMS.2014.09.008

[2] Zhang L, Brown T, Samuelsen S. Evaluation of charging infrastructure requirements and operating costs for plug-in electric vehicles. *J Power Sources*. 2013;240(2013): 515-524. DOI: 10.1016/J.JPOWSOUR.2013.04.048

[3] Rangarajua S, Vroeyb LD, Messagiea M, Mertensb J, Mierloa JV. Impacts of electricity mix, charging profile, and driving behavior on the emissions performance of battery electric vehicles: A Belgian case study. *Appl Energy*. 2015;148(2015):496-505. DOI: 10.1016/J.APENERGY.2015.01.121

[4] Neubauer J, Wood E. The impact of range anxiety and home, workplace, and public charging infrastructure on simulated battery electric vehicle lifetime utility. *J Power Sources*. 2014;257(2014):12-20. DOI: 10.1016/J.JPOWSOUR.2014.01.075

[5] Carreira D, Domingos Marques G, Sousa DM. Hybrid energy storage system joining batteries and supercapacitors. 2014 IEEE 5th International Symposium on Power Electronics for Distributed Generation Systems (PEDG); Jun 24-27; Galway. 2014. p. 1-6. DOI: 10.1109/PEDG.2014.6878712

[6] Doucette RT, McCulloch MD. A comparison of high-speed flywheels, batteries, and ultracapacitors on the bases of cost and fuel economy as the energy storage system in a fuel cell based hybrid electric vehicle. *J Power Sources*. 2011;196(3):1163-1170. DOI: 10.1016/J.JPOWSOUR.2010.08.100

[7] Li Q, Chena W, Li Y, Liu S, Hua J. Energy management strategy for fuel cell/battery/ ultracapacitor hybrid vehicle based on fuzzy logic. *Int J Electric Power Energy Sys*. 2012;43(1):514-525. DOI: 10.1016/J.IJEPES.2012.06.026

[8] Wang T, Deng W, Wu J, Zhang Q. Power optimization for hybrid energy storage system of electric vehicle. Transportation Electrification Asia-Pacific (ITEC Asia-Pacific), 2014 IEEE Conference and Expo; Aug 31-Sep 3; Beijing, China. 2014. p. 1-6. DOI: 10.1109/ITEC-AP.2014.6941224

[9] Guidi G, Undeland TM, Hori Y. Effectiveness of supercapacitors as power-assist in pure EV using a sodium-nickel chloride battery as main energy storage. EVS24; May 13-16; Stavanger, Norway. 2009. p. 1-9.

[10] He X, Parten M, Maxwell T, Energy management strategies for a hybrid electric vehicle. IEEE Conference on Vehicle Power and Propulsion; Sep 7-9; Chicago, USA. 2005. p. 536-540. DOI: 10.1109/VPPC.2005.1554610

[11] Ortuzar M, Moreno J, Dixon J. Ultracapacitor-based auxiliary energy system for an electric vehicle: implementation and evaluation. *IEEE Trans Indus Electron*. 2007;54(4): 2147 - 2156. DOI: 10.1109/TIE.2007.894713

[12] Cipollone R, Battista DD, Marchionni M, Villante C. Model based Design and Optimization of a Fuel Cell Electric Vehicle. *Energy Procedia*. 2014;45(2014):71-80. DOI: 10.1016/J.EGYPRO.2014.01.009

[13] Ansarey M, Panahib MS, Ziarati H, Mahjoob M. Optimal energy management in a dual-storage fuel-cell hybrid vehicle using multi-dimensional dynamic programming. *J Power Sources*. 2014;250(2014):359-371. DOI: 10.1016/J.JPOWSOUR.2013.10.145

[14] Woothipatanapan S, Jangwanitlert A, Chancharoensook P. Efficiency improvement of converter for switched reluctance motor drives by mixed parallel operation of IGBT and MOSFET. TENCON 2010 - 2010 IEEE Region 10 Conference; Nov.21-24; Fukuoka, Japan. 2010. p. 1841-1846. DOI: 10.1109/TENCON.2010.5685964

[15] Christen D, Tschannen S, Biela J. Highly efficient and compact DC-DC converter for ultra-fast charging of electric vehicles. 2012 15th International Power Electronics and Motion Control Conference (EPE/PEMC); Sep 4-6; Novi Sad, Serbia. 2012. p. LS5d. 3-1-LS5d.3-8. DOI: 10.1109/EPEPEMC.2012.6397481

[16] Bellar MD, Wu TS, Tchamdjou A, Mahdavi J, Ehsani M. A review of soft-switched DC-AC converters. *IEEE Trans Indus Applic*. Jul-Aug 1998;34(4):847-860. DOI: 10.1109/28.703992

[17] Tulbure A, Turschner D, Abrudean M, Ceuca E, Ormenisan R. Experimental comparation of switching with IGBT and MOSFET. Automation Quality and Testing Robotics (AQTR), 2010 IEEE International Conference on. 28-30 May 2010;2:1-5. DOI: 10.1109/AQTR.2010.5520804

[18] Abu-Rub H, Iqbal A, Guzinski J. Vector control of three-phase AC machines: *System Development in the Practice*. 1st ed. Verlag, Germany: Springer; 2008. 340 p. DOI: 10.1007/978-3-540-79029-7

[19] Dominic DA, Chelliah TR. Analysis of field-oriented controlled induction motor drives under sensor faults and an overview of sensorless schemes. *ISA Trans*. 2014;53(5):1680-1694. DOI: 10.1016/J.ISATRA.2014.04.008

[20] Rahman MF, Zhong L, Lim KW. A Direct torque-controlled interior permanent magnet synchronous motor drive incorporating field weakening. *IEEE Trans Indus Applic*. Nov/Dec 1998;34(6):1246-1253. DOI: 10.1109/28.738985

[21] Zhong L, Rahman MF, Hu WY, Lim KW. Analysis of direct torque control in permanent magnet synchronous motor drives. *IEEE Trans Power Electron*. May 1997;12(3): 528-536. DOI: 10.1109/63.575680

[22]   Bazzi A.M, Dominguez-Garcia A, Krein PT. Markov reliability modeling for induction motor drives under field-oriented control. *IEEE Trans Power Electron*. 2012;27(2): 534-546. DOI: 10.1109/TPEL.2011.2168543

[23]   Zeraoulia M, Benbouzid MEH, Diallo D. Electric motor drive selection issues for HEV propulsion systems: a comparative study. *IEEE Trans Vehicular Technol*. Nov. 2006;55(6):1756-1764. DOI: 10.1109/TVT.2006.878719

[24]   Morimoto S, Sanada M, Takeda Y. Wide-speed operation of interior permanent magnet synchronous motors with high-performance current regulator. *IEEE Trans Indus Applic*. Jul/Aug 1994;30(4):920-926. DOI: 10.1109/28.297908

[25]   Halder S, Srivastava SP, Agarwal P. Flux weakening control algorithm with MTPA control of PMSM drive. In: 2014 IEEE 6th India International Conference on Power Electronics (IICPE); Dec 8-10; Kurukshetra, India. 2014. p. 1-5. DOI: 10.1109/IICPE. 2014.7115810

[26]   Krishnan R. *Permanent Magnet Synchronous and Brushless DC Motor Drives*. Boca Raton, USA: CRC Press; 2009. 611 p. DOI: 10.1201/9781420014235-P3